# Local topological moves determine global diffusion properties of hyperbolic higher-order networks

Ana P. Millán [●],[1,*] Reza Ghorbanchian,[2] Nicolò Defenu [●],[3] Federico Battiston,[4] and Ginestra Bianconi [●][2,5]

[1]*Amsterdam UMC, Vrije Universiteit Amsterdam, Department of Clinical Neurophysiology and MEG Center,*
*Amsterdam Neuroscience, De Boelelaan 1117, Amsterdam, The Netherlands*
[2]*School of Mathematical Sciences, Queen Mary University of London, Mile End Road, E1 4NS, London, United Kingdom*
[3]*Institute for Theoretical Physics, ETH Zürich Wolfgang-Pauli-Str. 27, 8093 Zurich, Switzerland*
[4]*Department of Network and Data Science, Central European University, 1100 Vienna, Austria*
[5]*The Alan Turing Institute, British Library, 96 Euston Road, NW1 2DB, London, United Kingdom*

From social interactions to the human brain, higher-order networks are key to describe the underlying network geometry and topology of many complex systems. While it is well known that network structure strongly affects its function, the role that network topology and geometry has on the emerging dynamical properties of higher-order networks is yet to be clarified. In this perspective, the spectral dimension plays a key role since it determines the effective dimension for diffusion processes on a network. Despite its relevance, a theoretical understanding of which mechanisms lead to a finite spectral dimension, and how this can be controlled, still represents a challenge and is the object of intense research. Here, we introduce two nonequilibrium models of hyperbolic higher-order networks and we characterize their network topology and geometry by investigating the intertwined appearance of small-world behavior, $\delta$-hyperbolicity, and community structure. We show that different topological moves, determining the nonequilibrium growth of the higher-order hyperbolic network models, induce tuneable values of the spectral dimension, showing a rich phenomenology which is not displayed in random graph ensembles. In particular, we observe that, if the topological moves used to construct the higher-order network increase the area/volume ratio, then the spectral dimension continuously decreases, while the opposite effect is observed if the topological moves decrease the area/volume ratio. Our work reveals a new link between the geometry of a network and its diffusion properties, contributing to a better understanding of the complex interplay between network structure and dynamics.

## I. INTRODUCTION

Higher-order networks are generalized network structures that capture the many-body interactions of complex systems [1–6]. In recent years, they have become increasingly popular to represent different types of data beyond the framework of pairwise interactions, including the human brain [7–10], social interacting systems [11–19], financial networks [20,21], and complex materials [22–24]. Interestingly, several studies on synchronization, diffusion, epidemic spreading, and evolutionary dynamics have shown that taking into account the higher-order organization of networks can lead to emergent behavior remarkably different from that of graphs, where interactions are limited to groups of two nodes only [25–37]. Therefore, establishing the relation between the structure and the dynamics of higher-order networks is currently a field of intense research activity [2].

A powerful tool to characterize higher-order network data is topological data analysis, which provides a general mathematical and computational framework to analyze data from their topological shape [7,38–41]. In a number of cases, these analyses have been able to extract relevant information from real networks that cannot be detected by more traditional

Network Science metrics. Moreover, topology can directly affect higher-order network dynamics by determining the evolution of topological signals, i.e., dynamical signals defined not only on nodes but also on links, triangles, and other higher-order structures [25,42–44]. A natural way to represent higher-order networks is by simplicial complexes, which differently from graphs are not only formed by nodes and links, but also include triangles, tetrahedra and so on. Together with cell complexes—which allow as building blocks also other regular polytopes such as hypercubes and orthoplexes—simplicial complexes describe discrete topological spaces. Therefore, modeling higher-order networks with simplicial and cell complexes is often the first step for conducting a topological investigation of higher-order networks.

Models of dynamically evolving simplicial and cell complexes built by simple local rules can affect the higher-order network topology by causing the emergence of a nontrivial meso-scale topological organization. For instance, models of simplicial complexes implementing triadic closure [45], or constructed by gluing together simplices through the iteration of simple topological moves [23,24,46,47], were found to generate higher-order networks with emergent community structure. Moreover, simplicial complexes and cell complexes have also an intrinsic geometrical nature, and for this reason represent an ideal setting to investigate the properties of emergent hyperbolic network geometry in complex

*Corresponding author: a.p.millanvidal@amsterdamumc.nl

systems [4,23,24,46,48,49]. In particular, models of emergent hyperbolic network geometry reveal the fundamental rules responsible for the wide-spread occurrence of hyperbolicity in real network datasets and in the structure of knowledge graphs [50–54].

A characteristic feature of emergent geometries is revealed by the spectral properties of their network skeleton, i.e., the network that is generated from the higher-order system only retaining the pairwise interactions. In particular, a fundamental indication that the higher-order networks have a characteristic geometrical nature is associated with the emergence of a finite spectral dimension of their graph Laplacian. Broadly speaking, the spectral dimension $d_S$ of the graph Laplacian of a network indicates the dimension of the network as perceived by a random walker crawling on the network. As such, on a regular Euclidean lattice the spectral dimension $d_S$ coincides with the dimension of the lattice $d$.

Until recently, it was believed that the heterogeneous degree distributions and the Fiedler eigenvalue of the graph Laplacian were the main structural determinants for dynamical processes in networked systems. These considerations, however, reveal how the investigation of higher-order networks has recently transformed the way in which we look at the classical problem of the interplay between structure and dynamics on complex networks [55]. From the study of higher-order networks, it is now becoming clear that both network topology and network geometry can affect dynamics in unexpected ways that go well beyond previous beliefs [2]. In particular, the spectral dimension constitutes a fundamental quantity to capture how geometry affects dynamics. For instance, it is known to characterize the return time of random walkers [56,57], the stability of synchronized states [26,27], universal critical phenomena [58–64], quantum diffusion [65,66], or the universal properties of different quantum gravity approaches [67–69]. Remarkably, the value of the spectral dimension varies significantly from network to network. Moreover, in random graphs and expanders (i.e., sparse graphs with large Cheeger constant, which cannot be divided in two macroscopic subgraphs without cutting a large set of links [70,71]) the spectral dimension is not even defined as the highly nonlocal nature of their connections has the effect of introducing a spectral gap in the spectrum of the graph Laplacian.

Most of the models displaying emergent spectral dimension evolve by the iteration of simple topological moves that are also responsible for a nontrivial community structure. Moreover, in the existing models of emergent hyperbolic geometry that display a finite spectral dimension, including the model *Network Geometry with Flavor* [24,26,27,47], the dependence of the spectral dimension on the model parameters has yet to be clarified. Indeed, how a finite spectral dimension emerges is still an open problem. Which are the general microscopic mechanisms giving rise to a finite spectral dimension? What is its relation to hyperbolicity of the associated emergent geometries?

In this work we address these questions by systematically investigating the relation between the simple topological moves determining the local evolution of higher-order networks and their meso-scale and global properties. Our results are based on the analyses of two distinct classes of models—the short-range triadic closure (STC) model and the Network Geometry with Flavor (NGF) model—that generalize previous models enforcing triadic closure [45] and displaying emergent hyperbolic geometry [46], respectively. We illustrate how different local topological moves can lead to important differences in the large-scale structural and dynamical properties of the higher-order networks. Specifically, we show how different topological moves can be used to increase or decrease the value of the spectral dimension and the modularity of hyperbolic higher-order networks. Interestingly, we directly link the emergence of a smaller spectral dimension to topological moves that enforce a larger ratio between the area and the volume of the considered emergent hyperbolic geometries.

The paper is structured as follows. In Sec. II we define the two classes of models: the STC and the NGF model. In Sec. III we discuss the topological properties of these models, including a detailed discussion of the role of the topological moves on the evolution and emergence of nontrivial community structure in both models. In Sec. IV we characterize the emergent hyperbolic geometry of the STC and the NGF model. In Sec. V we show how the emergent spectral dimension of both models is modulated by the choice of topological moves adopted for the evolution of the higher-order network models and the implications for diffusion dynamics. Finally, in Sec. VI we provide some concluding remarks.

## II. HIGHER-ORDER NETWORK MODELS AND THEIR UNDERLYING NETWORK SKELETON

### A. Mathematical definition of cell complexes and network skeleton

Higher-order networks allow us to represent networked systems which are not limited to only pairwise interactions. A common way to describe such structures is to introduce new higher-order building blocks known as *simplices*. A $d$-dimensional simplex is formed by $d + 1$ nodes, each one interacting with all the other ones. Thus, a $d$-dimensional simplex is a node when $d = 0$, a link when $d = 1$, a triangle when $d = 2$, a tetrahedron when $d = 3$, and so on. The *faces* of a $d$-simplex are the simplices formed by a proper subset of its nodes. The underlying network skeleton of a $d$-simplex, i.e., the network retaining only the pairwise interactions between the nodes, is a $(d + 1)$-clique. *Simplicial complexes* — a collection of simplices which respect a particular inclusion rule of their lower order faces — provide a representation of higher-order networks. The *facets* of a simplicial complex are the simplices that are not faces of any other simplices of the simplicial complex. The *dimension* of a simplicial complex is the maximum dimension of its facets. The *skeleton* of a simplicial complex is the network constructed from the simplicial complex retaining only the information about its nodes and links.

In a number of real-world scenarios, however, higher-order networks may be constructed by building blocks which are more loosely connected than simplices. For instance, a protein interaction network is formed by a set of proteins that might have a complex interaction pattern involving more than two agents, but might not be binding to each other in all-to-all small subgraphs. These generalized building blocks

are know as *cells*. Mathematically, a $d$-dimensional cell is a $d$-dimensional convex polytope, i.e., a topological space homeomorphic to a $d$-dimensional open ball. Therefore, 0-dimensional cells are nodes and 1-dimensional cells are links, and thus do not differ from 0-dimensional and 1-dimensional simplices. However, differences originate in higher dimensions. For instance, 2-dimensional cells include $m$-polygons such as triangles (2-dimensional simplices), but also squares, pentagons, etc. Similarly, 3-dimensional cells include the Platonic solids, such as tetrahedra (3-dimensional simplices), cubes, octahedra, dodecahedra, and icosahedra. Interestingly, whereas in dimension $d = 4$ there are more regular polytopes than in dimension $d = 3$ (being 6), for any dimension $d > 4$ there are only three types of regular (convex) polytopes: the simplex, the hypercube and the orthoplex.

Similarly to simplicial complexes, cells may be aggregated into a cell complex. In particular, a cell complex $\hat{\mathcal{K}}$ has the following two properties:

(a) it is formed by a set of cells that is closure-finite, meaning that every cell is covered by a finite union of open cells;

(b) given two cells of the cell complex $\alpha \in \hat{\mathcal{K}}$ and $\alpha' \in \hat{\mathcal{K}}$, then either their intersection belongs to the cell complex, i.e., $\alpha \cap \alpha' \in \hat{\mathcal{K}}$ or their intersection is a null set, i.e., $\alpha \cap \alpha' = \emptyset$.

The dimension $d$ of a cell-complex is the maximum dimension of its cells. Therefore, a $d$-dimensional Euclidean square lattice can be seen as a cell-complex of dimension $d$ as it is formed by unit cells which are hypercubes of dimension $d$. Similar to simplicial complexes, the skeleton of a cell-complex is the network generated from the cell complex only retaining the pairwise interactions between its nodes.

### B. The building blocks of the proposed higher-order models

In the following we consider two nonequilibrium models of higher-order networks. Each model is characterized by the nonequilibrium dynamics describing the higher-order network growth. At each time step one or more nodes are added and connected to the rest of the network through a specific higher-order interaction, representing the building blocks of our networked structures, and taken to be either $d$-dimensional simplices or $d$-dimensional orthoplexes. The $d$-dimensional simplexes have been defined in the previous section as formed by $d + 1$ nodes, each one interacting with all the other ones. The $d$-dimensional orthoplex is a regular polytope with $2d$ nodes and $2^d$ faces formed by $(d - 1)$-dimensional simplices. For instance, in $d = 2$ the orthoplex is a square having 4 nodes and 4 links, for $d = 3$ the orthoplex is a bipyramid with a square basis having 6 nodes and 8 triangular faces. In general, the network skeleton of a collection of a $d$-dimensional orthoplex is more sparse than the one of $d$-dimensional simplices, which is a fully connected clique.

Since both $d$-simplices and $d$-orthoplexes admit as $(d - 1)$-faces exclusively $(d - 1)$-dimensional simplices, orthoplexes, and simplices can be easily glued to each other and combined as coexisting building blocks of a higher-order network (also called cell complex). For instance, in our higher-order network models defined in dimension $d = 2$, we will combine triangles and squares glued along their links in higher-order discrete architectures. However, $d$-simplices

and $d$-orthoplexes can be glued to each other according to different topological moves. To reveal the macroscopic consequences of the choice of different local moves, here we consider two specific models: the short-range triadic closure (STC) model, and a new variation of the network geometry with flavour (NGF) model proposed in Refs. [47,49].

### C. Short-range triadic closure (STC) model

The short-range triadic closure (STC) model is a higher-order network model that generalizes triadic closure models considering not only the introduction of triangles but also of squares. The model is defined as follows. Initially (at $t = 1$), the network is formed by an $(m + 1)$-clique with all its triangles filled. At each time step $t > 1$, a new node $r$ is added to the network and connected to the rest of the higher-order network by $m$ links and by $m - 1$ higher-order interactions. The first link of the new node is connected to a randomly selected node $i$. The remaining $m - 1$ links are chosen in such a way to close triangles with the first link $(r, i)$ with probability $q$, and to close squares with probability $1 - q$. If the first event occurs, then the new link is connected to a random neighbor $j$ of node $i$, forming the triangle $(r, i, j)$. On the contrary, if the second event occurs, then the new link is connected to a random second neighbor $j'$ of node $i$, a fourth node $k$ is selected among the common neighbors of $i$ and $j'$, and the square $(r, i, k, j')$ is formed. If $q = 1$, then the higher-order network grows exclusively by the addition of triangles, whereas for $q = 0$ it grows by the addition of squares. Therefore, the STC model generates cell complexes that are ($d = 2$)-dimensional. The process and the underlying network skeleton are illustrated in Fig. 1 for $m = 2$.

A long-range version of the model, without the limitation to connecting only to first or second neighbors, was extensively studied in Ref. [45]. It was shown to have a heavy-tailed degree distribution, short paths, a strong community structure and high clustering (for $q > 0$). The STC dynamics is only driven by an effective *sublinear* preferential attachment, i.e., new links are effectively attached to a generic node $i$ with a probability proportional to $k_i^\theta$ with $\theta < 1$; however, as $m$ increases the exponent $\theta$ approaches one, leading to broader degree distribution.

### D. The network geometry with flavor (NGF) model

The second model that we consider is a variation of the Network Geometry with Flavor (NGF) model proposed for cell complexes in Refs. [46,49]. In its original formulation, the NGF cell complexes evolved by the subsequent addition of a single type of regular polytope (i.e., all the polytopes of the cell complexes are the same). Here we generalize this modeling framework by allowing the cell complex to be formed by different types of $d$-dimensional polytopes. In particular, the present version of the NGF model generates $d$-dimensional higher-order networks by subsequently gluing together $d$-dimensional simplices, or $d$-dimensional orthoplexes, along their $(d - 1)$-faces. Each $(d - 1)$-face $\alpha$ of the higher-order network is characterized by its incidence number $n_\alpha$, indicating the number of $d$-dimensional polytopes incident to the face, minus 1.
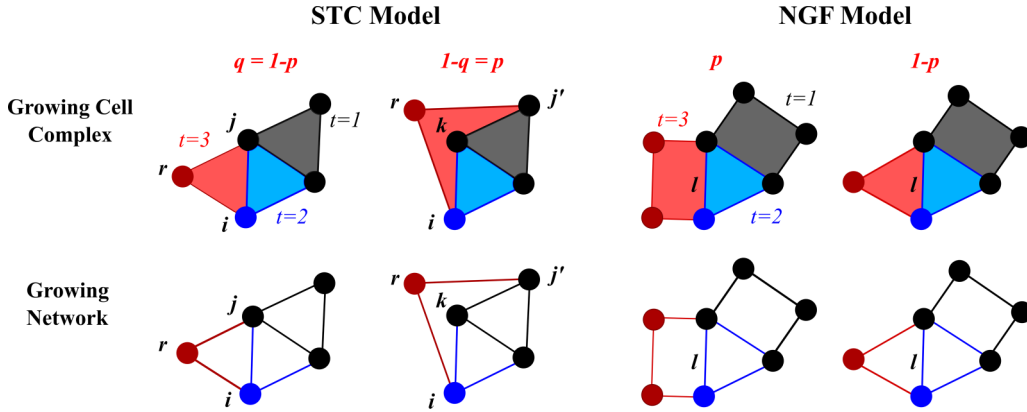
FIG. 1. Illustrative sketch of the different topological moves used to grow higher-order networks (top panels) for the STC (with $m = 2$) and NGF (with $d = 2$) models, and their corresponding network skeletons (bottom panels). In the case of the STC model, at each time an existing node $i$ is randomly selected. Then, with probability $q$ a first neighbor of node $i$, let us say node $j$, is randomly chosen, and a new node $r$ is linked to both $i$ and $j$, thus forming a triangle. By contrast, with probability $1 - q$ a second neighbor $j'$ of node $i$ is selected and the new node $r$ is linked to both $i$ and $j'$, closing a square. The fourth node $k$ conforming the square is randomly selected among the shared neighbors of $i$ and $j'$. For the NGF model, at each time-step an existing link $l$ is randomly selected according to Eq. (1) and either a square (with probably $p$) or a triangle (with probability $1 - p$) is added to the cell complex.

The higher-order network is constructed as follows. Initially (at $t = 1$), the NGF is formed by a single $d$-dimensional orthoplex. At every subsequent time step $t > 1$, a new $d$-dimensional polytope is glued to a $(d - 1)$-face $\alpha$. The new polytope is a $d$-dimensional orthoplex with probability $p$ and a $d$-dimensional simplex with probability $1 - p$. The face $\alpha$ to which the new polytope is attached is chosen with probability

$$\Pi_\alpha = \frac{1 + s n_\alpha}{\sum_{\alpha'} (1 + s n_{\alpha'})}, \tag{1}$$

where $s \in \{-1, 0, 1\}$ is a parameter of the NGF model called *flavor*. For $p = 0$, if we neglect the initial condition, the NGF is formed exclusively by $d$-dimensional simplices and reduces to the model treated in Ref. [49]. For $p = 1$, the NGF is formed exclusively by $d$-dimensional orthoplexes, and this limit has been studied in detail in Ref. [47].

In general, NGFs comprise of $d$-dimensional cell complexes. In the following, we will often refer to their network skeleton as the underlying NGF network. NGF networks display interesting combinatorial properties that have been well characterized in the case $p = 0$ [49] and $p = 1$ [47]: the degree distribution is scale-free for a wide range of values of $s$ and $d$, and the resulting networks are small-world and have an infinite Hausdorff dimension. Despite the small-world property, NGFs have a finite spectral dimension together with a strong hierarchical-modular community structure [27,47]. In this work we fix the value of the flavor of the NGF model to $s = 0$, leading to power-law networks as the result of an effective preferential attachment mechanism for any dimension $d \geqslant 2$. A schematic illustration of this model is also represented in Fig. 1 for $d = 2$.

## III. TOPOLOGICAL PROPERTIES OF THE STC AND THE NGF MODELS

The skeleton of the STC and NGF cell complexes — made up by considering only the nodes and links — makes up the STC and NGF networks, whose properties can be evaluated

through standard Network Science metrics. According to such type of analyses, the two models can be considered remarkably similar. They both lead to networks with high clustering, heterogeneous degree distributions, short paths and a strong community structure. For instance, we note the case of $m = 2$ (STC model) and $d = 2$ (NGF model). For $q = 1$ and $p = 0$, the two networks are made up by gluing triangles together. Then, as $q$ decreases (STC) or $p$ increases (NGF), triangles are substituted by squares. Thus, to compare the two models in the following, we define the complementary control parameter $p = 1 - q$ for the STC model, so that increasing $p$ leads in both models to a decrease in the number of triangles (or, more generally, simplices) and an increase in the number of squares (or orthoplexes) conforming the high-order network.

Despite the aforementioned similarities from the network science perspective, the two models are constructed by adopting different topological moves, as we go on to show in the following subsections.

### A. Topological moves for the STC and NGF model

The most striking difference between the STC and the NGF cell complexes is that, while the STC cell complex is $d = 2$ dimensional for every value of $m$, the NGF cell complex has varying dimension $d \geqslant 2$ given by the dimensionality of its building blocks. Besides, even if we limit our considerations only to STC and NGF cell complexes in dimension $d = 2$, the two models differ by the dynamical rules used for their generation. These rules, determining the way in which simplices and orthoplexes are added to the cell complex, are called in topology *topological moves*.

Both models share a remarkable feature, which is that the topological moves leading the evolution of the cell complexes do not change the topological invariants of the cell complexes. In fact, simplices and orthoplexes are added to the cell complex in such a way that neither the Betti numbers (with the only nonzero Betti number being $\beta_0 = 1$) nor the Euler characteristic of the cell complex $\chi$ change [72,73]. This

TABLE I. Changes in the number of nodes $\Delta V$, number of links $\Delta E$, and number of 2-dimensional cells $\Delta F$, and corresponding change in the Euler characteristic $\Delta \chi$ for each topological move determining the evolution of the STC and NGF high-order networks of dimension 2.

| Model | | Process | $+\Delta V$ | $-\Delta E$ | $+\Delta F$ | $\Delta \chi$ |
|---|---|---|---|---|---|---|
| STC | $m=2$ | Triangle | 1 | $-2$ | 1 | 0 |
| | | Square | 1 | $-2$ | 1 | 0 |
| | $m>2$ | 1$^{\text{st}}$ link | 1 | $-2$ | 1 | 0 |
| | | following links | 0 | $-1$ | 1 | |
| NGF | $d=2$ | Simplex | 1 | $-2$ | 1 | 0 |
| | | Orthoplex | 2 | $-3$ | 1 | 0 |



FIG. 2. Modularity $Q$ of the STC (a) and NGF (b) networks for different values of $m$ ($m = 2, \ 3, \ 4$ from top to bottom) and $d$ [$d = 2, \ 3, \ 4$ from top to bottom (at $p = 0$)]. Results are for $N = 10^3$. Shaded areas indicate margin errors and are given by the standard deviation; results are averaged over 100 network realizations.

latter property can be easily checked for both the STC and the NGF models in $d = 2$ using the well known definition of the Euler characteristic as alternating sum of the number $s_k$ of $k$-dimensional cells of the cell complex, with $0 \leqslant k \leqslant d$ [72,73] (leading, for $d = 2$, to the famous expression $\chi = V - E + F$ where $V$, $E$, and $F$ are, respectively, the number of nodes, links and 2-dimensional cells of the cell complex). For the STC model with $m = 2$, a single 2-dimensional cell is added at each time, which can be either a triangle glued to an existing link, or a square glued to two existing links. In both cases, the cell complex increases by one node, $\Delta V = 1$, two links, $\Delta E = 2$, and one two dimensional cell, $\Delta F = 1$, so the Euler characteristic changes by

$$\Delta \chi = \Delta V - \Delta E + \Delta F = 1 - 2 + 1 = 0. \quad (2)$$

For the STC model with $m > 2$, at each time, $m - 1$ cells of dimension $d = 2$ are added to the cell complex. The first cell is glued to a link as for the case $m = 2$, leading to $\Delta \chi = 0$. The subsequent cells share a link with the first cell (the one between the new node and the randomly chosen node) and add a new link, $\Delta E = 1$, and a 2-dimensional cell, $\Delta F = 1$, to the cell complex, where the 2-dimensional cell can be either a triangle or a square. Therefore, none of the subsequently added cells change the Euler characteristic of the cell complex either, i.e.,

$$\Delta \chi = \Delta V - \Delta E + \Delta F = 0 - 1 + 1 = 0. \quad (3)$$

In the case of the NGF model, for $d = 2$ at each time we add a single 2-dimensional cell glued to a single link. If the added cell is a triangle, then this adds a single node, $\Delta V = 1$, two links, $\Delta E = 2$, and one triangle, $\Delta F = 1$, leading to

$$\Delta \chi = \Delta V - \Delta E + \Delta F = 1 - 2 + 1 = 0. \quad (4)$$

If, on the contrary, the added 2-dimensional cell is a square, then it adds two new nodes, $\Delta V = 2$, three links, $\Delta E = 3$, and one square, $\Delta F = 1$, leading to

$$\Delta \chi = \Delta V - \Delta E + \Delta F = 2 - 3 + 1 = 0. \quad (5)$$

By similar direct inspection it can be easily shown that also for dimensions $d > 2$ the topological moves that define the NGF evolution do not change the Euler characteristic. The changes of $\Delta V$, $\Delta E$, $\Delta F$, and $\Delta \chi$ for all the discussed topological moves are summarized in Table I.
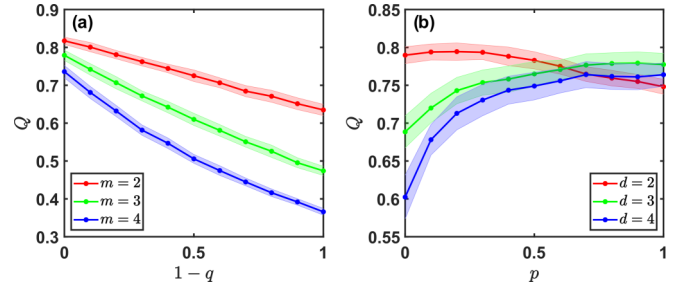
### B. Emergent community structure

*Triadic closure* was recently proposed as a general, unifying mechanism to generate a community structure [45]. Such a process is frequently observed in social networks, where open triads are often closed over time, and the density of triangles is remarkably high [74–76]. Models of network growth based on simple triadic closure have been shown [45] to naturally lead to the emergence of community structure, provided that the network is sufficiently sparse.

Interestingly, the nonequilibrium mechanisms leading to the emergence of a community structure are at work both in the STC and NGF models via the local topological moves. Consequently, both models lead to network skeletons with a strong community structure, as indicated by the high values of the modularity coefficient $Q$ (see Fig. 2). However, as $p$ increases the models display radically different behaviors: for STC networks $Q$ decays almost linearly with $p = 1 - q$, whereas for NGF networks with $d = 3$ and 4, it grows. In the STC model, as longer-range connections become more prominent, interconnections between regions also grow, decreasing the modularity. By contrast, orthoplexes in the NGF model are less interconnected with the rest of the network, as they only share one face with it, but have more faces than simplices, leading to an increase in the modularity. In this perspective, the NGF model with $d = 2$ stands out as its behavior is more complex: the modularity is relatively high for all $p$, following an inverse U-shape. In any case, the value of the modularity of the NGF model remains always significantly high, in contrast to the STC model.

## IV. EMERGENT GEOMETRICAL NETWORK PROPERTIES

### A. Infinite Hausdorff dimension

In this section we discuss the emergent geometrical properties of the STC and the NGF networks. An important geometrical notion that applies to network models with variable number of nodes, including regular lattices, is that of the Hausdorff dimension. The Hausforff dimension describes how the mean distance of the network $\ell$ scales with the total number of nodes (or network size) $N$, as $N$ goes to infinity. $\ell$ is defined as

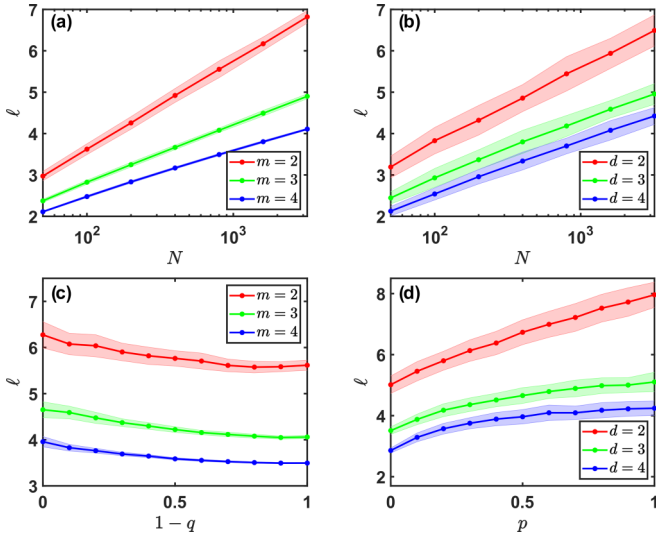$$\ell = \frac{1}{N(N-1)} \sum_{i} \sum_{j \neq i} d_{ij}, \quad (6)$$

FIG. 3. We represent the mean minimum path $\ell$ for the STC (panel (a)) and NGF (panel (b)) networks as a function of the network size $N$ for $p = 0.5$. $\ell$ grows logarithmically with $N$, which is indicative of the small-world property. Panels (c) and (d) show $\ell$ for different values of $m$ and $d$, respectively for the STC and NGF models, for networks with $N = 10^3$ nodes. Results in all panels have been averaged over a set of 100 network realizations, and the shaded areas indicate the error margins as given by the standard deviation.

where $d_{ij}$ is the length of the minimum path between nodes $i$ and $j$. For regular lattices, the mean distance on the network scales as a power of the network size for $N \gg 1$,

$$\ell \sim N^{1/d_H}, \tag{7}$$

where $d_H$ is the *Hausdorff dimension*. In most random graphs, like Erdös-Rényi ones, $\ell$ scales logarithmically with the size $N$, i.e., $\ell \sim \log N$, meaning that distances on the network are short, and it is possible to go from one node to any other passing through a small number of intermediate nodes. This is the so-called *small-world* property, which corresponds to an infinite Hausdorff dimension,

$$d_H = \infty. \tag{8}$$

Both the STC and NGF models are small-world and have an infinite Hausdorff dimension, as shown in Figs. 3(a) and 3(b). However, for a fixed value of $N$, the characteristic distance $\ell = \ell(N)$ behaves remarkably differently in the STC and NGF models as a function, respectively, of $q$ and $p$ as it is shown in Figs. 3(c) and 3(d). In fact, in the STC model, as $p = 1 - q$ increases and we add more squares, distances in the network decrease as longer distance links become more common. This is evidenced by the decrease in the characteristic distance $\ell$ with $p = 1 - q$ [see Fig. 3(c)]. On the contrary, distances on the NGFs networks increase as more orthoplexes are added (with increasing $p$), for any dimension $d$ [see Fig. 3(d)]. To better interpret this finding, we note that orthoplexes have more faces than simplices, and they are only glued to the existing network through one of them, *de facto* increasing distances on the network.
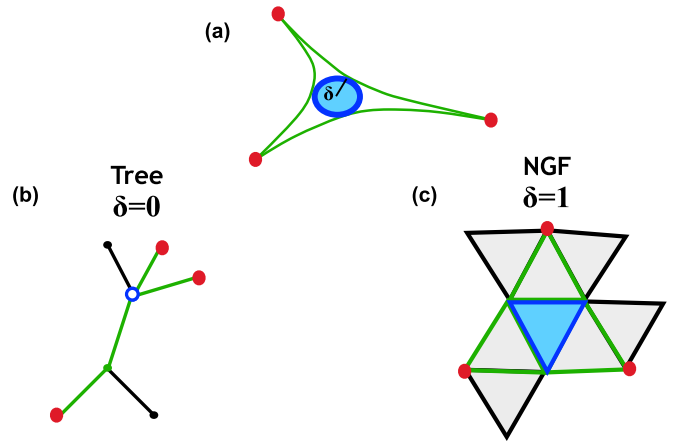


FIG. 4. Schematic representation of $\delta$-hyperbolicity. (a) Schematic representation of a $\delta$-thin triangle formed by three nodes of the network and the shortest paths between the nodes. (b) Hyperbolic tree with $\delta = 0$. To calculate the $\delta$-hyperbolicity, we select a triad of nodes (red bold dots) and calculate the shortest paths among them. For a tree, these intersect (at least) in one node (blue empty node), and so the distance is always $\delta = 0$. (c) NGF network ($d = 2$, $p = 0$) with $\delta = 1$. For the NGF network, the three paths do not intersect in general, but they are at a maximum distance $\delta = 1$. Note that in this case all the paths intersect in one triangle (shown in blue/dark) and so the NGF networks can be seen as trees of polytopes.

### B. $\delta$-hyperbolicity of the STC and the NGF models

Hyperbolicity is an important geometrical aspect of real-world networks, and it is know to affect the efficiency of search [78], the efficacy of embedding algorithms [53,54], and the behavior of dynamical processes such as percolation [79].

An important principle to test the hyperbolicity of real networks was proposed by Gromov [50], who formulated the concept of $\delta$-hyperbolicity of networks [23,24,51,52]. The $\delta$-hyperbolicity measures how far a network is from a hyperbolic tree by comparing the structure of shortest paths of triads of nodes on the network. On a tree these paths always share at least one vertex, i.e., they are at distance $\delta = 0$ and the tree is $\delta = 0$ hyperbolic [77]. However, more in general the paths need not touch and the distance among them may be finite. This defines the *fatness* of the triad. Hyperbolic spaces are characterized by having thin triangles (small $\delta \ll N$). These concepts are illustrated in Fig. 4. Interestingly, in a number of real networks $\delta$ remains always small, and in particular much smaller than the network diameter, indicating the hyperbolic geometry of the network.

Here, to characterize the $\delta$-hyperbolicity of the STC and the NGF model we adopt the so-called four-point criterion [51]. We consider any quadruple of distinct nodes $(i_1, i_2, i_3, i_4)$ of the networks, and we choose their permutation $(u_1, u_2, u_3, u_4) = i_{\pi(1)}, i_{\pi(2)}, i_{\pi(3)}, i_{\pi(4)}$ such that the following inequalities hold,

$$S_{u_1,u_2,u_3,u_4} \leqslant M_{u_1,u_2,u_3,u_4},$$
$$M_{u_1,u_2,u_3,u_4} \leqslant L_{u_1,u_2,u_3,u_4}, \tag{9}$$

where $d_{u,v}$, is the distance between the node pair $(u, v)$, as defined above, and $S_{u_1,u_2,u_3,u_4}$, $M_{u_1,i_2,u_3,u_4}$ and $L_{u_1,i_2,u_3,u_4}$ are
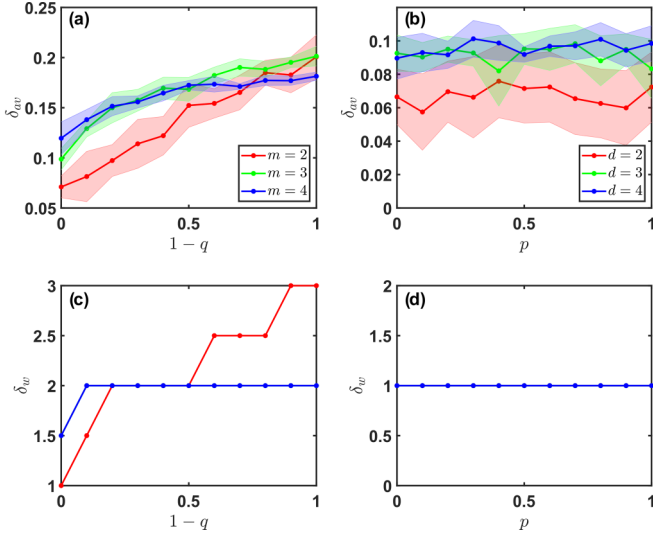
FIG. 5. The $\delta$-hyperbolicity of the STC and the NGF models is revealed by plotting the average $\delta_{av}$ for the STC model (panel a) and for the NGF model (panel b) and the worst value $\delta_w$ [panel (c) for the STC networks with $m = 2$, 3, 4 from bottom to top (at $1 - q = 0$), and panel (d) for the NGF networks with $d = 2$, 3, 4 from bottom to top (at $p = 1$)]. In panel (c) the curve for $m = 3$ overlays with the one for $m = 4$, whereas in panel (d) all the curves ($d = 2$, 3, 4) overlay.

defined as

$$S_{u_1,u_2,u_3,u_4} = d_{u_1,u_2} + d_{u_3,u_4},$$
$$M_{u_1,u_2,u_3,u_4} = d_{u_1,u_3} + d_{u_2,u_4},$$
$$L_{u_1,u_2,u_3,u_4} = d_{u_1,u_4} + d_{u_2,u_3}. \tag{10}$$

For any quadruple of nodes $(i_1, i_2, i_3, i_4)$, once we have found their permutation $(u_1, u_2, u_3, u_4)$ satisfying Eq. (9) we define

$$\delta^+_{i_1,i_2,i_3,i_4} = \tfrac{1}{2}[L_{u_1,u_2,u_3,u_4} - M_{u_1,u_2,u_3,u_4}]. \tag{11}$$

To evaluate the $\delta$-hyperbolicity of the network, we consider two metrics: the $\delta_w$ or worst (largest) value of $\delta^+$, and the average value of $\delta^+$, $\delta_{av}$, which are defined as

$$\delta_w = \max_{(i_1,i_2,i_3,i_4)} \delta^+_{i_1,i_2,i_3,i_4},$$

$$\delta_{av} = \left[ \binom{N}{4} \right]^{-1} \sum_{i_1,i_2,i_3,i_4} \delta^+_{i_1,i_2,i_3,i_4}. \tag{12}$$

Both the STC and the NGF networks are $\delta$-hyperbolic, as shown in Fig. 5. In particular, the NGF has a constant value of $\delta_w = 1$, which implies that the short-paths are either at distance 0 or 1, i.e., they always share at least one polytope. Thus, NGFs can be interpreted as "trees of polytopes" as exemplified in Fig. 4(c). For STC networks, on the contrary, $\delta_w$ can be greater than one. To determine the $\delta$-hyperbolic structure of STC networks, we follow Ref. [77], where it was proposed to characterize the $\delta$-hyperbolicity of finite networks by comparing it to the network diameter $D$, as a function of the number of edges in the network $E$. This is depicted in Figs. 6 and 7, respectively, for the average value $\delta_{av}$ and for the worst value $\delta_w$. The results indicate that, in the large network limit, both $\delta_{av}/(D/2)$ and $\delta_w/(D/2)$ decrease with the network size, illustrating the $\delta$-hyperbolicity of these higher-order network
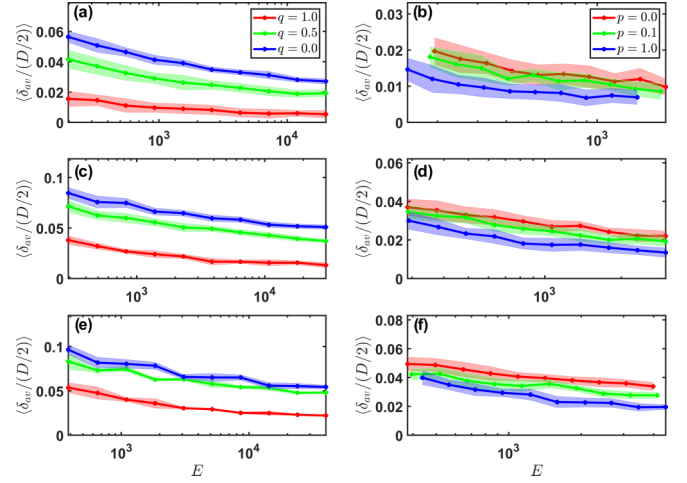


FIG. 6. The normalized quantity $\delta_{av}/(D/2)$, where $D$ indicates the network diameter, is plotted versus the number of links $E$ of the network. Panels (a, c, e) correspond to STC networks with $m = 2$, 3, 4, respectively, and $q$ as indicated by the legend ($q = 1.0$, 0.5, 0.0 from bottom to top, in each panel). Panels (b, d, f) correspond to NGF networks with $d = 2$, 3, 4, respectively, and $p$ as indicated by the legend ($p = 0.0$, 0.1, 1.0 from top to bottom, in each panel). Each data-point indicates the average over 20 network realizations, with the shaded error bars indicating the standard deviation. For each network, $\delta_{av}$ is estimated by randomly sampling over $10^7$ node quadruplets [77].
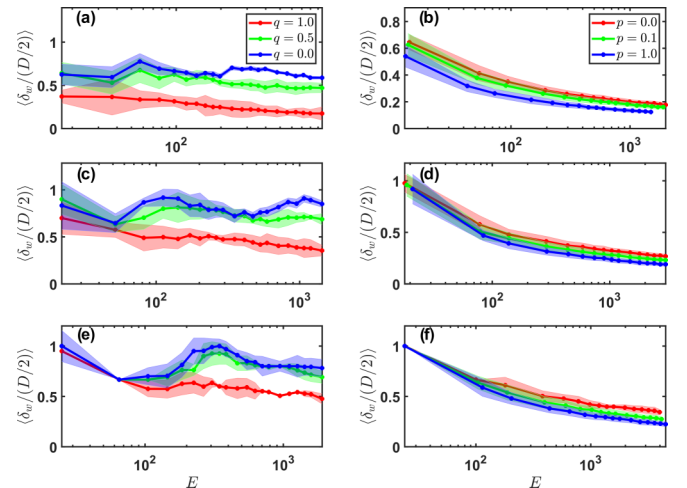


FIG. 7. The normalized quantity $\delta_w/(D/2)$, where $D$ indicates the network diameter, is plotted versus the number of links $E$ of the network, for STC (a, c, e) and NGF (b, d, f) networks with $m, d = 2$, 3, 4 from top to bottom and $q$ and $p$ as indicated by the legends [$q = 1.0$, 0.5, 0.0 from bottom to top, and $p = 0.0$, 0.1, 1.0 from top to bottom, in each panel, respectively for the STC and NGF models] [77]. Curves for STC networks with $q < 1$ (particularly for $m = 3$ and 4) display a nontrivial transient behavior due to (i) the small network sizes and (ii) the initial condition for the network consisting in one simplex without any second-neighbors, which leads to transient fluctuations on the effective value of $q$, noticeable for the small network sizes considered here. After this transient, $\delta_w/(D/2)$ decreases again in all cases.

models. We note that an exact calculation of $\delta_{\text{av}}$ and $\delta_w$ is highly computationally demanding (since all network quadruplets need to be examined) which prohibits the examination of very large network sizes. Thus, results in Fig. 6 for $\delta_{\text{av}}$ are obtained by subsampling the space possible quadruplets [77], whereas results in Fig. 7 for $\delta_w$ (the maximum value which cannot be accurately estimated by subsampling) correspond to small network sizes which can be fully explored.

Moreover, for both models we found that $\delta_{\text{av}} \ll \delta_w$, indicating that in general the distance between the shortest paths is much smaller than the maximum given by $\delta_w$. These results confirm that both the STC and NGF (with flavor $s = 0$) models define emergent hyperbolic network geometries, even tough these are not discrete manifolds [since in general the incidence number of the $(d - 1)$-dimensional faces ($d = 2$ always for the STC model] can be greater than 1, in which case different $d$-dimensional cells associated with a face intersect]. Note that, while the STC remains $\delta$-hyperbolic for any value of the parameter $q$, the model in Ref. [45] allowing each new node to connect with nonzero probability to two or more nodes chosen randomly in the network is not $\delta$-hyperbolic.

### C. Area and volume of STC and NGF models

The ratio between the area $A$ and the volume $V$ of the cell-complexes generated by the STC and NGF models is also a very notable geometrical property of the considered models which is a further indication of their hyperbolicity. For reference, it is useful to refer to known results valid for Euclidean and hyperbolic manifolds (even tough the considered STC and NGF models do not define manifolds). For Euclidean balls of radius $R$, the area $A$ and the volume $V$ are given by [80]

$$A = \Omega_d R^{d-1}, \quad V = \frac{\Omega_d}{d} R^d, \tag{13}$$

where

$$\Omega_d = \frac{2\pi^{d/2}}{\Gamma(d/2)}. \tag{14}$$

Therefore, the area and volume of a ball with unitary radius, $A = \Omega_d$ and $V = \Omega_d/d$, depend nontrivially on the dimension of the ball $d$. In particular, they have a nonmonotonic behavior, with the volume having a maximum for $d^\star \simeq 5.25$ and the area having a maximum for $d^\dagger \simeq 7.25$ (see Fig. 8). Therefore, for high dimension $d$ both the area and the volume of the unit ball decrease with $d$. More in general, the area-volume ratio of a ball of radius $R$ is given by

$$\frac{A}{V} = \frac{d}{R}. \tag{15}$$

Therefore, the ratio $A/V$ vanishes to zero in the limit of a ball of large radius, i.e., $A/V \to 0$ for $R \to \infty$.

A different behavior is observed for hyperbolic manifolds. For $\mathbb{H}^d$ hyperbolic manifolds in dimension $d$ [81], a ball of radius $R$ in $\mathbb{H}^d$ has area and volume given by

$$A = \Omega_d \sinh^{d-1}(R),$$

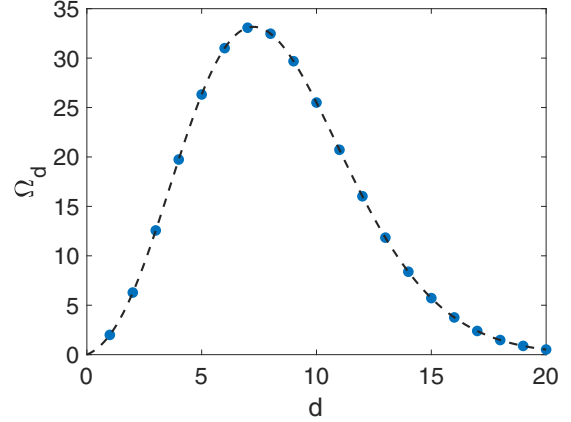$$V = \Omega_d \int_0^R \sinh^{d-1}(x)\,dx, \tag{16}$$



FIG. 8. The area $A = \Omega_d$ of a unit ball in $d$ dimension is plotted versus $d$ and is shown to display a nonmonotonous behavior with a maximum for $d^\dagger \simeq 7.25$.

with $\Omega_d$ given always by Eq. (14). Thus, the scaling with $R$ changes and in this case the area-volume ratio remains finite in the $R \to \infty$ limit, i.e.,

$$\lim_{R \to \infty} \frac{A}{V} = d - 1. \tag{17}$$

Let us now explore the area-to-volume ratio in the STC and the NGF models. We define the area $A$ of a $d$-dimensional cell complex which is pure, (i.e., whose facets are all polytopes of dimension $d$) as given by the number of $(d - 1)$-dimensional faces $\alpha$ that are incident to a single polytope (or equivalently with incidence number $n_\alpha = 0$). Similarly, we define the volume $V$ of a $d$-dimensional cell complex which is pure, as the total number its $(d - 1)$-dimensional faces.

Since the STC model is a $d = 2$ dimensional cell complex for every value of $m$, its area $A$ is given by the number of links which are incident either to a single triangle or to a single square. The volume $V$ of the STC is given by the total number of links. For the NGF model in dimension $d$, the area $A$ is the number of $(d - 1)$-simplices of the cell complex that are incident to a single $d$-dimensional cell (either a $d$-dimensional orthoplex or a $d$-dimensional simplex). The volume $V$ of the NGF is given by the total number of $(d - 1)$-simplices.
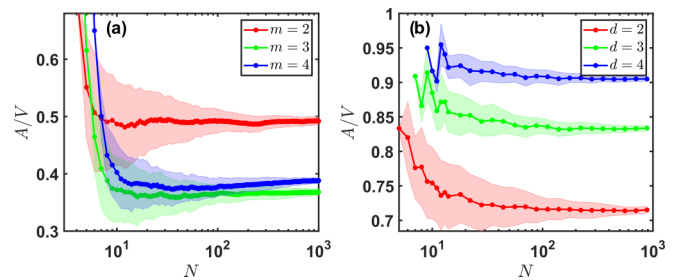


FIG. 9. We illustrate the convergence of $A/V$ during network growth for the STC (a) and NGF (b) models, for different values of $m$ [$m = 2$, 4, 3 from top to bottom (for large N)] and $d$ [$d = 2$, 3, 4 from bottom to top], and for $q = p = 0.5$. In all panels, results are averaged over 100 network realizations, and the shaded areas indicate the error margins as given by the standard deviation.

We are now in place to study the dependence with the network size of the ratio $A/V$ for the STC and NGF models. As it can be seen from Fig. 9, the ratio $A/V$ reaches a constant value in the large network limit, confirming the hyperbolic nature of the models. As shown in Figs. 13(c) and 13(d), the limiting value of the ratio $A/V$ depends on the value of $q$ (for the STC model) and $p$ (for the NGF model), even tough the dimension $d$ of the cell complex is independent of $q$ and $p$. Therefore, the ratio $A/V$ does not give an indication of the dimension $d$. In the next section we will show how the value of $A/V$ can be related instead to a different notion of dimension, the spectral dimension of the network.

## V. SPECTRAL DIMENSION AND DIFFUSION DYNAMICS

Much information on the structure of a network is given by the properties of its associated Laplacian matrix [56,82]. For many complex networks, the Fiedler (second smallest) eigenvalue remains finite in the thermodynamic limit (the smallest eigenvalue is zero by definition), and in such case the network is said to display a *spectral gap*. On the contrary, if the spectral gap closes as the system size grows, then the network is said to have a finite spectral dimension when the scaling of the cumulative density of eigenvalues of the Laplacian follows a power law [56,83,84].

Here we consider the normalized Laplacian **L** with elements

$$L_{ij} = \delta_{ij} - \frac{a_{ij}}{k_j}, \qquad (18)$$

where $a_{ij}$ is the adjacency matrix of the network and $\delta_{ij}$ is the Kronecker's delta. **L** has real nonnegative eigenvalues $0 = \lambda_1 \leqslant \lambda_2 \leqslant ... \leqslant \lambda_N$. The spectral density $\rho(\lambda)$ indicating the

density of eigenvalues is defined as

$$\rho(\lambda) = \frac{1}{N} \sum_{i=1}^{N} \delta(\lambda, \lambda_i), \qquad (19)$$

where $\delta(x, y)$ indicates the delta function. If the second smallest eigenvalue $\lambda_2$ goes to zero in the large network limit, i.e., $\lambda_2 \to 0$ for $N \to \infty$, and the density of eigenvalues $\rho(\lambda)$ for $\lambda \ll 1$ scales as

$$\rho(\lambda) \simeq C\lambda^{d_S/2-1}, \qquad (20)$$

with $C$ indicating a constant, we say that the network has *spectral dimension* $d_S$. The spectral dimension $d_S$ also characterizes the scaling of the spectral gap (given by $\lambda_2$) with the network size as

$$\lambda_2(N) \simeq C'N^{-2/d_S}. \qquad (21)$$

The spectral dimension can be interpreted as the dimension of the network as perceived by a random walker (RW) diffusing on it, and it is a notable feature of networks with a distinct geometrical nature. For Euclidean lattices in dimension $d$, the spectral dimension coincides with the Hausdorff dimension, i.e., $d_S = d_H = d$. However, in general networks the spectral dimension can strongly differ from the Hausdorff dimension [85,86].

As we go on to show, both the STC model and the NGF model display a finite spectral dimension $d_S \geqslant 2$ for most of their parameter values, which coexists with their infinite Hausdorff dimension $d_H = \infty$. This spectral dimension can be tuned by changing the control parameters $q$ and $p$, respectively, in the STC and in the NGF model. In particular, the spectral dimension of STC networks increases for larger
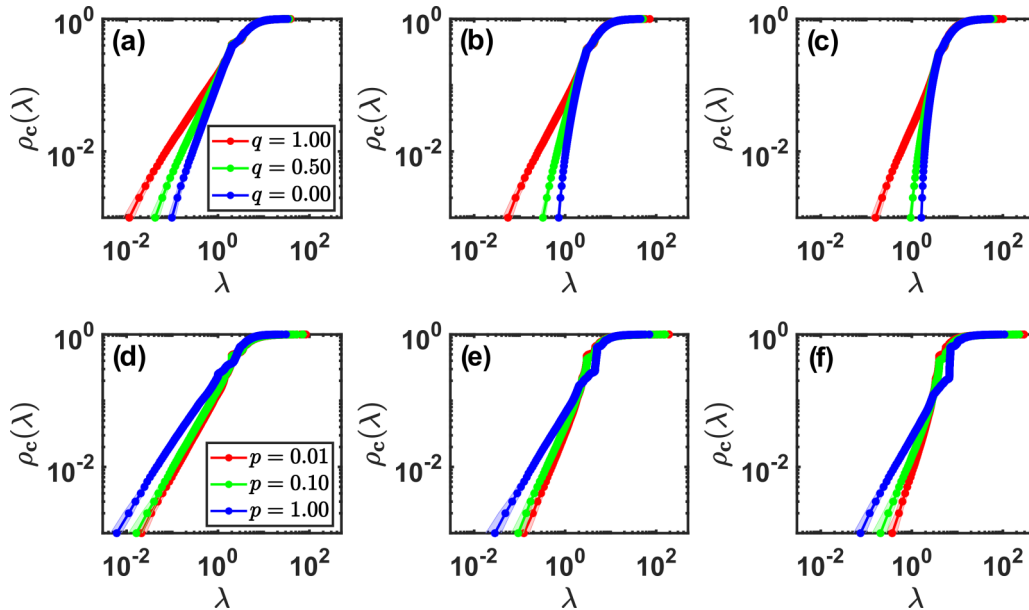


FIG. 10. The cumulative density $\rho_c(\lambda)$ of eigenvalues $\lambda$, is shown for the STC [panels (a), (b), and (c), respectively, for $m = 2, 3, 4$] and the NGF models [panels (d), (e), and (f), respectively, for $d = 2, 3, 4$]. We have used networks with $N = 10^3$ and parameters $p$ and $q$ shown in the legends ($q = 1.00\ 0.50,\ 0.00$ from left to right (panels a-c); $p = 0.01,\ 0.10,\ 1.00$ from right to left (panels d-f)]. The data has been averaged over 100 network realizations. The error margins as indicated by the standard deviation are shown with shaded areas (although in most cases the error area overlaps with the data-points).
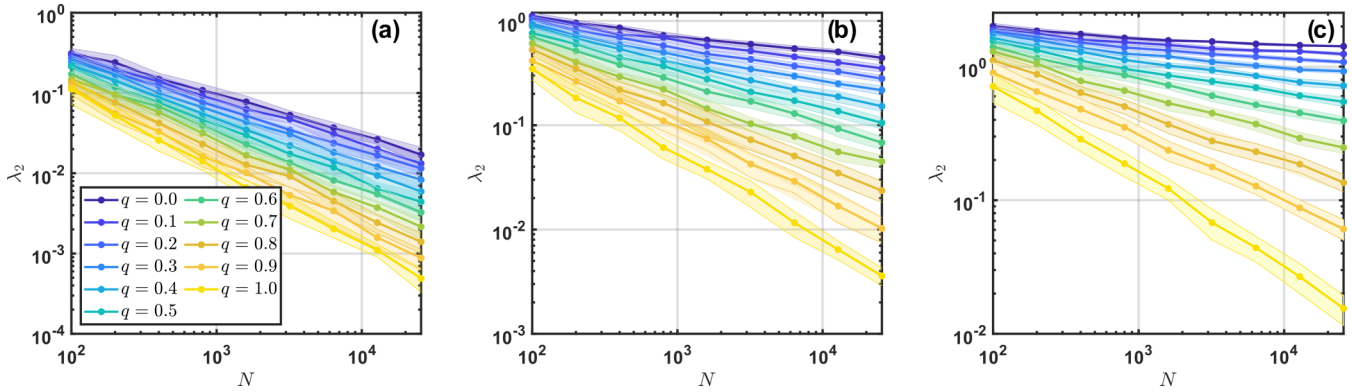
FIG. 11. The spectral gap $\lambda_2$ of STC networks is plotted versus the number of nodes $N$ for $m = 2$ (panel a), $m = 3$ (panel b) and $m = 4$ (panel c) and for different values of $q$ as indicated in the legend. Results correspond to $N = 10^3$ and have been averaged over 20 network realizations. The shaded regions indicate the error as given by the standard deviation.

values of $p = 1 - q$, while $d_S$ decreases for NGF networks with larger values of $p$.

To provide evidence for this effect, in Fig. 10 we show the cumulative spectral density $\rho_c(\lambda)$ for STC and NGF networks for a choice of the values $q$ and $p$, respectively. In presence of a finite spectral dimension $d_S$, $\rho_c(\lambda)$ should scale as a power law for $\lambda \ll 1$, i.e.,

$$\rho_c(\lambda) \simeq C'' \lambda^{d_S/2}, \tag{22}$$

where $C''$ is a constant. For NGF networks $d_S$ is well-defined $\forall \, (d, p)$ pairs [47], as confirmed by the power-law scaling of $\rho_c(\lambda)$ in Figs. 10(d)–10(f). In particular, $d_S$ decreases [i.e., the slope of $\rho_c(\lambda)$ is less pronounced] in a nonlinear manner as $p$ is increases (see below). Notably, NGF networks also present some degenerate eigenvalues in the high portion of the spectrum, due to the underlying network symmetries.

For the STC model, the scaling of $\rho_c(\lambda)$, Figs. 10(a)–10(c), indicates that the spectral dimension increases as $q$ decreases (see below). Notably, it also shows that the spectral gap increases with $d$ and with decreasing $q$. Thus, we have measured $\lambda_2(N, d, q)$, as shown in Fig. 11. We have found that a power-law decay of $\lambda_2$, $\lambda_2 \sim N^{-\gamma}$, $\gamma > 0$, is compatible with the observed data for all $(m, q)$, indicating that the spectral gap closes in the infinite network limit, and that the spectral dimension is well defined. To further validate these results, in Fig. 12 we have compared the two estimations of the spectral dimension: $d_S^{[1]}$ as given by the scaling of $\rho_c(\lambda)$, and $d_S^{[2]}$ as given by the scaling of $\lambda_2(N)$, by measuring the difference $\Delta d_S(m, q) = d_S^{[1]}(m, q) - d_S^{[2]}(m, q)$. As shown in the figure, both procedures yield very similar results as long as $d_S \lesssim 6$. For larger $d_S$ values the error in the estimation of $d_S$ grows, due to the finite network size, and the two measures may differ, but their difference remains within error bars.

In summary, we have found that the spectral dimension of STC and NGF networks behaves in opposite ways with $p$: it grows (in an approximately linear manner for $d_S < 6$) for STC networks, whereas it decreases (in a nonlinear manner) for NGF networks [see Figs. 13(a) and 13(b)]. This result shows that, by changing the local topological moves by which the higher-order network skeleton evolves, it is possible to tune the corresponding value of the spectral dimension. In

particular, our results show that, in the considered hyperbolic higher-order network models, a smaller $d_S$ corresponds to a larger ratio $A/V$ between the area and the volume of the cell complex [see Figs. 13(c) and 13(d)]. Therefore, the ratio $A/V$ of the STC and NGF models is not indicative of their topological dimension, but rather it correlates with the spectral dimension $d_S$. This indicates that the different choice of topological moves used to generate the higher-order networks can at the same time change the area/volume ratio of the hyperbolic STC and NGF models and tune the value of their spectral dimension.

To illustrate how a different network structure and geometry affect the dynamical properties of the networks, we have explicitly considered the diffusion dynamics of random walkers on the STC and NGF networks. Given a set of random walkers diffusing on a network, the return-time probability $P_0(t)$ is defined as the probability that a walker is back at its
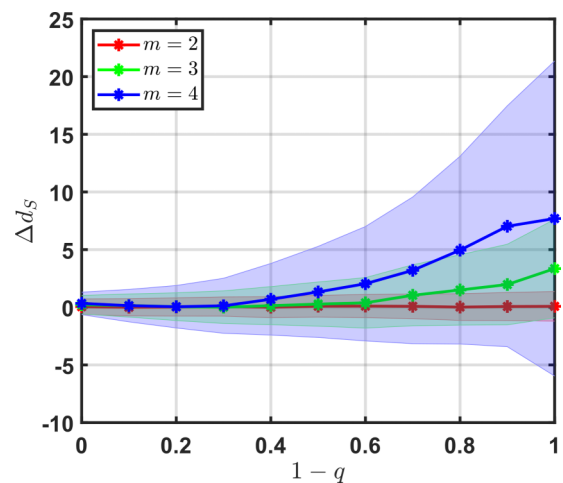


FIG. 12. Analysis of the estimation of the spectral dimension $d_S$ for the STC model. We compare the $d_S$ fits obtained from $\rho_c(\lambda)$, $d_S^{[1]}$, as in Fig. 13, and from $\lambda_2(N)$, $d_S^{[2]}$, by measuring $\Delta d_S = d_S^{[1]} - d_S^{[2]}$. Data corresponds to STC networks with $m = 2$ (red, bottom curve), 3 (green, middle curve), and 4 (blue, top curve). As it can be shown, as $1 - q \to 1$, $\Delta d_S$ grows for $m = 4$ and, to a lesser extend, for $m = 3$. However, the difference is compatible with 0.
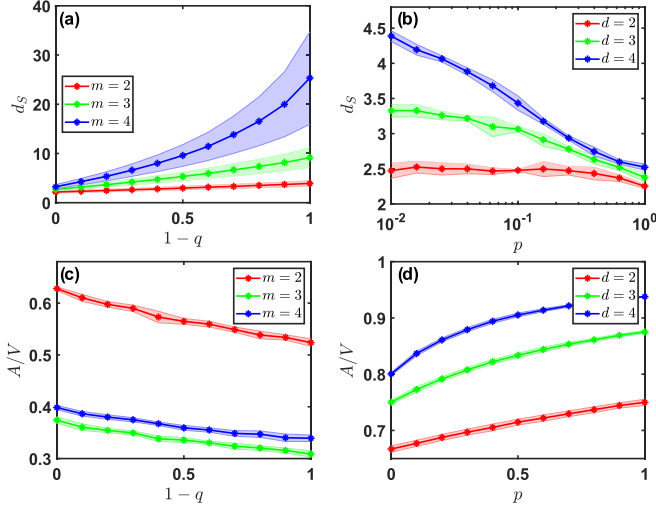
FIG. 13. We show the spectral dimension $d_S$ as a function of $p$ for STC [$m = 2$, 3, 4, from bottom to top panel (a), $p = 1 - q$] and NGF [$s = 0$, $d = 2$, 3, 4, from bottom to top panel (b)] networks. The values were measured from the $\rho_c(\lambda)$ curves as illustrated in Fig. 10 using aggregated data from 400 networks. The error bars indicate the confidence intervals. The determination of $d_S$ gets less reliable for increasing values of $d_S$, as the cutoff for the power-law fit becomes more pronounced. Panels (c) and (d) show the area-volume ratio $A/V$, respectively, for the STC and NGF models, for $m$ and $d$ as indicated in the legends [$m = 2$, 3, 4 from top to bottom (panel c); $d = 2$, 3, 4 from bottom to top (panel d)].

initial position at time $t$. This is directly linked to the spectral density by the equation [87]

$$P_0(t) = \int_0^\infty d\lambda e^{-\lambda t} \rho(\lambda). \tag{23}$$

As a consequence, for networks with a finite spectral dimension, the return-time probability distribution decays as a power law for $t \gg 1$, $t < t_{\text{cut}}$, where $t < t_{\text{cut}}$ is the cutoff time
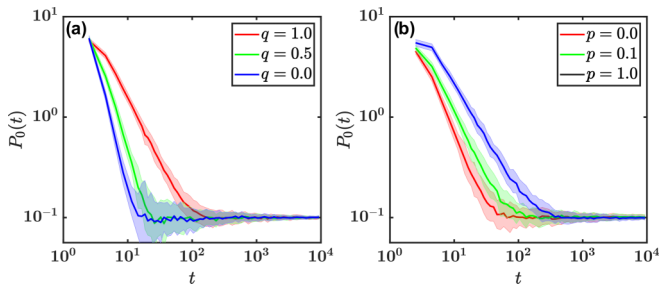


FIG. 14. Return-time probability $P_0(t)$ of the random walk for STC networks with $m = 4$ and $q = 1.0$, 0.5, 0.0 from right to left (a) and NGFs with $d = 4$, $s = 0$ and $p = 0.0$, 0.1, 1.0 from left to right (b), and $N = 10^3$. Results are measured over 50 realizations of the networks, and 20 realizations of the RW dynamics for each network. Initially, $N_{\text{RW}} = 10^3$ walkers are placed on the network at randomly selected nodes $n_i$, $i = 1, \ldots, N_{\text{RW}}$. At each time step, each walker jumps with uniform probability to one of the neighbors of $n_i$, independently of the other walkers' positions. This process is iterated for $T_{\text{RW}} = 10^4$ steps, and the return-time probability $P_0(t)$ that a walker returns to its starting point after $t$ steps is measured.

due to finite-size effects, with power-law exponent determined by the spectral dimension, i.e.,

$$P_0(t) \propto t^{-d_S/2}. \tag{24}$$

This relation reveals the role of the spectral dimension as a key spectral property, explicitly linking the structural and dynamical properties of a network.

By performing explicit simulations of the random walk dynamics, we have measured the return-time probability $P_0(t)$ for STC and NGF networks (see Fig. 14). These results confirm that the spectral dimension of the STC and the NGF models can be tuned by varying the parameter $q$ (for the STC model) and $p$ (for the NGF) model.

## VI. CONCLUSIONS

Higher-order networks allow us to properly encode and investigate complex systems where interactions are not limited to two nodes at a time. In particular, their characterization beyond traditional metrics from statistical mechanics and network science reveals new features of the complex interplay between network structure and dynamics.

In this work we proposed a general nonequilibrium framework which makes it possible to obtain tunable emergent hyperbolic network geometries, and provide new insights on how topology and geometry affect diffusion dynamics. We introduced two models, namely, the STC and NGF higher-order models, which are generated by iteration of simple, local, topological moves. We investigated how variations in these local rules are reflected in the geometrical properties of the higher-order networks. In particular, despite leaving the topological invariants of the higher-order network unchanged, we showed that local moves have the ability to modify the emerging geometrical and diffusion properties; see Sec. III. We measured the diffusion properties of the considered models in terms of their spectral dimension, a remarkable geometrical property of their network skeleton that determines the return-time probability distribution of a random walk crawling on it. We found that the spectral dimension can be tuned continuously on the considered models by modulating the ratio between the area and the volume of the higher-order models, explicitly governed by the choice of the topological moves. In particular, as the area-volume ratio decreases, the spectral dimension of the model increases. The considered models of emergent network geometries are also found to show other nontrivial features of real-world systems, including the small-world property, $\delta$-hyperbolicity, and significant community structure. We believe that our work reveals a new link between the geometry of a network and the properties of diffusion processes taking place on top of it, contributing at a fundamental level to a better understanding of the complex interplay between network structure and dynamics.

## ACKNOWLEDGMENTS

[1] F. Battiston, G. Cencetti, I. Iacopini, V. Latora, M. Lucas, A. Patania, J.-G. Young, and G. Petri, Networks beyond pairwise interactions: Structure and dynamics, Physics Reports **874**, 1 (2020).

[2] G. Bianconi, *Higher-order Networks: An Introduction to Simplicial Complexes* (Cambridge University Press, Cambridge, UK, 2021).

[3] L. Torres, A. S. Blevins, D. S. Bassett, and T. Eliassi-Rad, The why, how, and when of representations for complex systems, SIAM Review **63**, 435 (2021).

[4] G. Bianconi, Interdisciplinary and physics challenges of network theory, Europhys. Lett. **111**, 56001 (2015).

[5] V. Salnikov, D. Cassese, and R. Lambiotte, Simplicial complexes and complex systems, Eur. J. Phys. **40**, 014001 (2018).

[6] C. Giusti, R. Ghrist, and D. S. Bassett, Two's company, three (or more) is a simplex, J. Comput. Neurosci. **41**, 1 (2016).

[7] G. Petri, P. Expert, F. Turkheimer, R. Carhart-Harris, D. Nutt, P. J. Hellyer, and F. Vaccarino, Homological scaffolds of brain functional networks, J. R. Soc., Interface **11**, 20140873 (2014).

[8] M. W. Reimann, M. Nolte, M. Scolamiero, K. Turner, R. Perin, G. Chindemi, P. Dłotko, R. Levi, K. Hess, and H. Markram, Cliques of neurons bound into cavities provide a missing link between structure and function, Front. Comput. Neurosci. **11**, 48 (2017).

[9] B. Tadić, M. Andjelković, and R. Melnik, Functional geometry of human connectomes, Sci. Rep. **9**, 12060 (2019).

[10] E. G. Z. Centeno, G. Moreni, C. Vriend, L. Douw, and F. A. N. Santos, A hands-on tutorial on network and topological neuroscience, bioRxiv (2021).

[11] G. Petri and A. Barrat, Simplicial Activity Driven Model, Phys. Rev. Lett. **121**, 228301 (2018).

[12] I. Iacopini, G. Petri, A. Barrat, and V. Latora, Simplicial models of social contagion, Nat. Commun. **10**, 2485 (2019).

[13] N. W. Landry and J. G. Restrepo, The effect of heterogeneity on hypergraph contagion models, Chaos: An Interdisciplinary J. Nonlin. Sci. **30**, 103117 (2020).

[14] G. St-Onge, H. Sun, A. Allard, L. Hébert-Dufresne, and G. Bianconi, Bursty Exposure on Higher-Order Networks Leads to Nonlinear Infection Kernels, Phys. Rev. Lett. **127**, 158301 (2021).

[15] B. Jhun, M. Jo, and B. Kahng, Simplicial sis model in scale-free uniform hypergraph, J. Stat. Mech.: Theory Exp. (2019) 123207.

[16] G. F. de Arruda, G. Petri, and Y. Moreno, Social contagion models on hypergraphs, Phys. Rev. Research **2**, 023032 (2020).

[17] T. Carletti, F. Battiston, G. Cencetti, and D. Fanelli, Random walks on hypergraphs, Phys. Rev. E **101**, 022308 (2020).

[18] J. T. Matamalas, S. Gómez, and A. Arenas, Abrupt phase transition of epidemic spreading in simplicial complexes, Phys. Rev. Research **2**, 012049(R) (2020).

[19] G. Cencetti, F. Battiston, B. Lepri, and M. Karsai, Temporal properties of higher-order interactions in social networks, Sci. Rep. **11**, 7028 (2021).

[20] M. Tumminello, T. Aste, T. Di Matteo, and R. N. Mantegna, A tool for filtering information in complex systems, Proc. Natl. Acad. Sci. USA **102**, 10421 (2005).

[21] G. P. Massara, T. Di Matteo, and T. Aste, Network filtering for big data: Triangulated maximally filtered graph, J. Complex Netw. **5**, 161 (2016).

[22] D. S. Bassett, E. T. Owens, K. E. Daniels, and M. A. Porter, Influence of network topology on sound propagation in granular materials, Phys. Rev. E **86**, 041306 (2012).

[23] M. Šuvakov, M. Andjelković, and B. Tadić, Hidden geometries in networks arising from cooperative self-assembly, Sci. Rep. **8**, 1987 (2018).

[24] M. M. Dankulov, B. Tadić, and R. Melnik, Spectral properties of hyperbolic nanonetworks with tunable aggregation of simplexes, Phys. Rev. E **100**, 012309 (2019).

[25] A. P. Millán, J. J. Torres, and G. Bianconi, Explosive Higher-Order Kuramoto Dynamics on Simplicial Complexes, Phys. Rev. Lett. **124**, 218301 (2020).

[26] A. P. Millán, J. J. Torres, and G. Bianconi, Complex network geometry and frustrated synchronization, Sci. Rep. **8**, 9910 (2018).

[27] A. P. Millán, J. J. Torres, and G. Bianconi, Synchronization in network geometries with finite spectral dimension, Phys. Rev. E **99**, 022307 (2019).

[28] R. Ghorbanchian, J. G. Restrepo, J. J. Torres, and G. Bianconi, Higher-order simplicial synchronization of coupled topological signals, Commun. Phys. **4**, 120 (2021).

[29] P. S. Skardal and A. Arenas, Abrupt Desynchronization and Extensive Multistability in Globally Coupled Oscillator Simplexes, Phys. Rev. Lett. **122**, 248301 (2019).

[30] M. Lucas, G. Cencetti, and F. Battiston, Multiorder Laplacian for synchronization in higher-order networks, Phys. Rev. Research **2**, 033410 (2020).

[31] R. Mulas, C. Kuehn, and J. Jost, Coupled dynamics on hypergraphs: Master stability of steady states and synchronization, Phys. Rev. E **101**, 062313 (2020).

[32] U. Alvarez-Rodriguez, F. Battiston, G. F. de Arruda, Y. Moreno, M. Perc, and V. Latora, Evolutionary dynamics of higher-order interactions in social networks, Nature Human Behaviour **5**, 586 (2021).

[33] A. Salova and R. M. DSouza, Cluster synchronization on hypergraphs, arXiv:2101.05464 (2021).

[34] Á. Bodó, G. Y. Katona, and P. L. Simon, Sis epidemic propagation on hypergraphs, Bull. Math. Biol. **78**, 713 (2016).

[35] G. Burgio, A. Arenas, S. Gómez, and J. T. Matamalas, Network clique cover approximation to analyze complex contagions through group interactions, Commun. Phys. **4**, 111 (2021).

[36] X. Dai, K. Kovalenko, M. Molodyk, Z. Wang, X. Li, D. Musatov, A. Raigorodskii, K. Alfaro-Bittner, G. Cooper, G. Bianconi *et al.*, D-dimensional oscillators in simplicial structures: Odd and even dimensions display different synchronization scenarios, Chaos, Solitons Fractals **146**, 110888 (2021).

[37] G. Burgio, J. T. Matamalas, S. Gómez, and A. Arenas, Evolution of cooperation in the presence of higher-order in-

teractions: From networks to hypergraphs, Entropy **22**, 744 (2020).

[38] N. Otter, M. A. Porter, U. Tillmann, P. Grindrod, and H. A. Harrington, A roadmap for the computation of persistent homology, EPJ Data Sci. **6**, 17 (2017).

[39] A. P. Kartun-Giles and G. Bianconi, Beyond the clustering coefficient: A topological analysis of node neighborhoods in complex networks, Chaos, Solitons Fractals: X **1**, 100004 (2019).

[40] Y. Lee, J. Lee, S. M. Oh, D. Lee, and B. Kahng, Homological percolation transitions in evolving coauthorship complexes, Chaos **31**, 041102 (2021).

[41] O. Bobrowski and P. Skraba, Homological percolation and the euler characteristic, Phys. Rev. E **101**, 032304 (2020).

[42] D. Taylor, F. Klimm, H. A. Harrington, M. Kramár, K. Mischaikow, M. A. Porter, and P. J. Mucha, Topological data analysis of contagion maps for examining spreading processes on networks, Nat. Commun. **6**, 7723 (2015).

[43] S. Barbarossa and S. Sardellitti, Topological signal processing over simplicial complexes, IEEE Trans. Signal Process. **68**, 2992 (2020).

[44] J. J. Torres and G. Bianconi, Simplicial complexes: Higher-order spectral dimension and dynamics, J. Phys.: Complex. **1**, 015002 (2020).

[45] G. Bianconi, R. K. Darst, J. Iacovacci, and S. Fortunato, Triadic closure as a basic generating mechanism of communities in complex networks, Phys. Rev. E **90**, 042806 (2014).

[46] G. Bianconi and C. Rahmede, Emergent hyperbolic network geometry, Sci. Rep. **7**, 41974 (2017).

[47] D. Mulder and G. Bianconi, Network geometry and complexity, J. Stat. Phys. **173**, 783 (2018).

[48] Z. Wu, G. Menichetti, C. Rahmede, and G. Bianconi, Emergent complex network geometry, Sci. Rep. **5**, 10073 (2015).

[49] G. Bianconi and C. Rahmede, Network geometry with flavor: From complexity to quantum geometry, Phys. Rev. E **93**, 032315 (2016).

[50] M. Gromov, in *Essays in Group Theory* (Springer, Berlin, 1987), pp. 75–263.

[51] R. Albert, B. DasGupta, and N. Mobasheri, Topological implications of negative curvature for biological and social networks, Phys. Rev. E **89**, 032811 (2014).

[52] O. Narayan and I. Saniee, Large-scale curvature of networks, Phys. Rev. E **84**, 066108 (2011).

[53] I. Chami, R. Ying, C. Ré, and J. Leskovec, Hyperbolic graph convolutional neural networks, Adv. Neural Info. Process. Syst. **32**, 4869 (2019).

[54] I. Chami, A. Wolf, D.-C. Juan, F. Sala, S. Ravi, and C. Ré, Low-dimensional hyperbolic knowledge graph embeddings, arXiv:2005.00545 (2020).

[55] S. N. Dorogovtsev, A. V. Goltsev, and J. F. F. Mendes, Critical phenomena in complex networks, Rev. Mod. Phys. **80**, 1275 (2008).

[56] R. Burioni and D. Cassi, Universal Properties of Spectral Dimension, Phys. Rev. Lett. **76**, 1091 (1996).

[57] N. Masuda, M. A. Porter, and R. Lambiotte, Random walks and diffusion on networks, Phys. Rep. **716**, 1 (2017).

[58] G. S. Joyce, Spherical model with long-range ferromagnetic interactions, Phys. Rev. **146**, 349 (1966).

[59] S. Bradde, F. Caccioli, L. Dall'Asta, and G. Bianconi, Critical Fluctuations in Spatial Complex Networks, Phys. Rev. Lett. **104**, 218701 (2010).

[60] E. Aygün and A. Erzan, Spectral renormalization group theory on networks, in *Journal of Physics: Conference Series* (IOP Publishing, Bristol, UK, 2011) Vol. 319, p. 012007.

[61] N. Defenu, A. Trombettoni, and A. Codello, Fixed-point structure and effective fractional dimensionality for O(N) models with long-range interactions, Phys. Rev. E **92**, 052113 (2015).

[62] N. Defenu, A. Trombettoni, and S. Ruffo, Criticality and phase diagram of quantum long-range O(N) models, Phys. Rev. B **96**, 104432 (2017).

[63] G. Gori, M. Michelangeli, N. Defenu, and A. Trombettoni, One-dimensional long-range percolation: A numerical study, Phys. Rev. E **96**, 012108 (2017).

[64] A. P. Millán, G. Gori, F. Battiston, T. Enss, and N. Defenu, Complex networks with tuneable spectral dimension as a universality playground, Phys. Rev. Research **3**, 023015 (2021).

[65] O. Mülken and A. Blumen, Continuous-time quantum walks: Models for coherent transport on complex networks, Phys. Rep. **502**, 37 (2011).

[66] J. Nokkala, J. Piilo, and G. Bianconi, Probing the spectral dimension of quantum network geometries, J. Phys.: Complex. **2**, 015001 (2020).

[67] J. Ambjørn, J. Jurkiewicz, and R. Loll, The Spectral Dimension of the Universe is Scale Dependent, Phys. Rev. Lett. **95**, 171301 (2005).

[68] D. Benedetti, Fractal Properties of Quantum Spacetime, Phys. Rev. Lett. **102**, 111303 (2009).

[69] G. Calcagni, A. Eichhorn, and F. Saueressig, Probing the quantum nature of spacetime by diffusion, Phys. Rev. D **87**, 124028 (2013).

[70] C. Moore and S. Mertens, *The Nature of Computation* (Oxford University Press, Oxford, UK, 2011).

[71] S. Hoory, N. Linial, and A. Wigderson, Expander graphs and their applications, Bull. Amer. Math. Soc. **43**, 439 (2006).

[72] H. Edelsbrunner, A short course in computational geometry and topology, in *Mathematical Methods* (Springer, Berlin, 2014).

[73] R. W. Ghrist, *Elementary Applied Topology* Vol. 1 (Createspace, Seattle, 2014).

[74] M. E. Newman and J. Park, Why social networks are different from other types of networks, Phys. Rev. E **68**, 036122 (2003).

[75] R. Toivonen, J.-P. Onnela, J. Saramäki, J. Hyvönen, and K. Kaski, A model for social networks, Physica A **371**, 851 (2006).

[76] D. V. Foster, J. G. Foster, P. Grassberger, and M. Paczuski, Clustering drives assortativity and community structure in ensembles of networks, Phys. Rev. E **84**, 066117 (2011).

[77] E. Jonckheere, P. Lohsoonthorn, and F. Bonahon, Scaled Gromov hyperbolic graphs, J. Graph Theory **57**, 157 (2008).

[78] R. Kleinberg, Geographic routing using hyperbolic space, in *Proceedings of the 26th IEEE International Conference on Computer Communications (INFOCOM'07)* (IEEE, Piscataway, NJ, 2007), pp. 1902–1909.

[79] I. Kryven, R. M. Ziff, and G. Bianconi, Renormalization group for link percolation on planar hyperbolic manifolds, Phys. Rev. E **100**, 022306 (2019).

[80] K. Huang, *Introduction to Statistical Physics* (CRC Press, Boca Raton, FL, 2009).

[81] J. G. Ratcliffe, *Foundations of Hyperbolic Manifolds*, Vol. 149 (Springer, Berlin, 2006).

[82] R. Rammal, Random walk statistics on fractal structures, J. Stat. Phys. **36**, 547 (1984).

[83] R. Burioni, D. Cassi, and A. Vezzani, Inverse Mermin-Wagner theorem for classical spin models on graphs, Phys. Rev. E **60**, 1500 (1999).

[84] S. Hwang, C.-K. Yun, D.-S. Lee, B. Kahng, and D. Kim, Spectral dimensions of hierarchical scale-free net-works with weighted shortcuts, Phys. Rev. E **82**, 056110 (2010).

[85] T. Jonsson and J. F. Wheater, The spectral dimension of the branched polymer phase of two-dimensional quantum gravity, Nucl. Phys. B **515**, 549 (1998).

[86] B. Durhuus, T. Jonsson, and J. F. Wheater, The spectral dimension of generic trees, J. Stat. Phys. **128**, 1237 (2007).

[87] A. Barrat, M. Barthelemy, and A. Vespignani, *Dynamical Processes on Complex Networks* (Cambridge University Press, Cambridge, UK, 2008).